

TDOA-based localization with NLOS mitigation via robust model transformation and neurodynamic optimization

Wenxin Xiong^{a,*}, Christian Schindelhauer^a, Hing Cheung So^b, Joan Bordoy^a,
Andrea Gabbrielli^a, Junli Liang^c

^a*Department of Computer Science, University of Freiburg, Freiburg 79110, Germany*

^b*Department of Electrical Engineering, City University of Hong Kong, Hong Kong, China*

^c*School of Electronics and Information, Northwestern Polytechnical University, Xi'an
710072, China*

Abstract

This paper revisits the problem of locating a signal-emitting source from time-difference-of-arrival (TDOA) measurements under non-line-of-sight (NLOS) propagation. Many currently fashionable methods for NLOS mitigation in TDOA-based localization tend to solve their optimization problems by means of convex relaxation and, thus, are computationally inefficient. Besides, previous studies show that manipulating directly on the TDOA metric usually gives rise to intricate estimators. Aiming at bypassing these challenges, we turn to retrieve the underlying time-of-arrival framework by treating the unknown source onset time as an optimization variable and imposing certain inequality constraints on it, mitigate the NLOS errors through the ℓ_1 -norm robustification, and finally apply a hardware realizable neurodynamic model based on the redefined augmented Lagrangian and projection theorem to solve the resultant nonconvex optimization problem with inequality constraints. It is validated through extensive simulations that the proposed scheme can strike a nice balance between localization accuracy, computational complexity, and prior knowledge require-

*Corresponding author

Email addresses: w.x.xiong@outlook.com (Wenxin Xiong),
schindel@informatik.uni-freiburg.de (Christian Schindelhauer), hcco@ee.cityu.edu.hk
(Hing Cheung So), bordoy@informatik.uni-freiburg.de (Joan Bordoy),
andre_gabe@hotmail.it (Andrea Gabbrielli), liangjunli@nwpu.edu.cn (Junli Liang)

ment.

Keywords: Source localization, non-line-of-sight, time-difference-of-arrival, robust model transformation, neural network, nonconvex optimization

1. Introduction

Source localization using measurements from spatially separated passive sensors has turned into a go-to scheme in many location-based services including target tracking [1, 2], human-computer interaction [3], and Internet of Things [4]. Among plentiful measurement models, the time-of-arrival (TOA) and time-difference-of-arrival (TDOA), especially the latter that eliminates the need for synchronization between the source and sensors [5, 6, 7, 8], is perhaps the most widely used owing to its high accuracies. For an insight into the rationale of single source localization, the uninitiated readers are referred to [9, 10] and the references therein.

One of the key issues in source localization is the so-called non-line-of-sight (NLOS) propagation, which commonly arises in real environments (e.g., urban canyons and indoor sites), and can adversely degrade the positioning performance if left untreated [10, 11, 12, 13, 14, 15, 16, 17, 18, 19, 20, 21]. Over the past decade, a vast variety of advanced NLOS mitigation methods have been developed for TOA-based localization: the worst-case least squares (LS) [11], joint estimation of the source location and a balancing parameter [12, 13, 14], and robust multidimensional similarity analysis [15], to name a few. These approaches are practically more favorable than the straightforward maximum likelihood (ML) technique [16], as their implementations rely on neither the path status nor the specified error distribution, but merely a few assumptions regarding the measurement noise and/or NLOS errors. Different from what one might expect, extension of the aforementioned TOA-based schemes to the TDOA case is not at all a trivial task. This is mainly because the possible NLOS error in a TDOA measurement is essentially the difference of those occurred in two related TOA measurements, and hence may not necessarily be a

positive outlier anymore. To settle this matter, the authors of [17] follow again the worst-case rule, but this time the upper bound is imposed on the magnitude of NLOS errors. As a modification to [17] which treats each measurement equally, additional path status information is utilized in [18] for placing less reliance on the error-prone measurements. More recently, the authors of [19] point out that the formulations in [17] and [18] may not perform well due to the loose upper bound and inexact triangle inequality, whereupon they put forward several refinements to alleviate the impacts. Despite considerable resistance of the worst-case criterion to NLOS errors, solving the resultant robust LS problems in [17, 18, 19], however, involves the use of convex optimization such as second-order cone programming (SOCP) and semidefinite programming (SDP), which will bring in heavy computational burdens. On the other hand, whereas the TDOA model with a structure more complex than the TOA counterpart can impede the formulation derivation [22], the idea of model transformation is suggested in [20, 23]. Such a tactic is well-motivated to the extent that the metrics of TOA and TDOA differ by only one degree of freedom, i.e., the time at which the signal departs from the source. Moreover, the selection of a proper reference sensor is no longer a prerequisite after the model transformation. Nevertheless, the constrained LS estimator with NLOS mitigation in [20] still ends up with solving a complicated SDP problem.

Conventional numerical methods for optimization are often realized and run on digital computers. Consequently, the computing time can grow dramatically with the increase of problem size, implying less effectiveness in time-varying scenarios. To overcome this drawback, employing physically implementable recurrent neural networks by which distributed, parallel, and real-time computation is enabled has become a promising alternative for tackling various classes of mathematical programming problems [24, 25, 26, 27, 28, 29, 41]. The mechanism is to build a dynamical system that will ultimately settle down to an equilibrium point, at which the optimal solution to the problem is obtained from the outputs, given suitable inputs as the initial point. In particular, the Lagrange programming neural networks (LPNN) [24] developed based on the gradient

model [26] and Lagrange multiplier theory has provided a general framework for coping with the nonlinear constrained optimization problems. With the use of an augmented Lagrangian function, the LPNN model can further be empowered to handle nonconvex optimization, and recent studies have successfully utilized the augmented LPNN to solve a mass of source localization problems [30, 31, 32, 33, 34]. However, the standard LPNN framework is unfriendly towards the presence of inequality constraints, since it requires introducing slack variables to convert them into the equality ones as a preprocessing step. This is apparently not a fine option if a large number of inequality constraints are involved, in view of the fact that promptness and real-time responses are the main purposes of applying the recurrent neural networks. Unfortunately, for the sake of binding the additional nuisance variable, there do exist many inequality constraints in the model transformation approaches [20], which indicates that a more efficient means of neurodynamic optimization is still a yearning in our application.

In this paper, we formulate TDOA-based source localization in NLOS environments as a nonconvex constrained optimization problem by robust model transformation, and then devise an effective and efficient neurodynamic solution to it. To start with, the least absolute deviation (LAD) (also known as (a.k.a.) the ℓ_1 -norm) criterion is adopted to achieve robustness against the bias-like NLOS error in the reconstructed TOA measurement model. For the higher-order properties in the design of dynamical system, certain smoothed approximations are made to the LAD objective function to yield a twice differentiable surrogate. Unlike most of the neurodynamic source localization approaches adapting their formulations to the standard LPNN setting (e.g., by either discarding the inequality constraints [30, 32] or transforming them into the equalities [31, 33, 34]), we follow [28] to redefine the augmented Lagrangian and establish a different projection-type neural network (PNN) model which can directly take the inequality constraints into account. It is worth noting that although the LPNN and PNN share the same terminology “neural network” with the booming deep neural networks in machine learning, they refer to to-

tally distinct approaches and should not be mixed up with each other. The presented scheme obviates the need for acquiring any information (e.g., an upper bound [17, 18, 19]) concerning NLOS errors or tuning the hyperparameters [20] beforehand, thereby resulting in a lower prior knowledge demand compared to the methods in [17, 18, 19, 20]. It should be noted that though bearing some resemblance to [20] which also remodels the problem into a TOA framework, our work should be distinguished from it, as neither the ℓ_2 -space-based objective function nor the time-consuming SDP is counted on any longer. In addition, our neurodynamic solution is shown to be computationally more efficient even when it is executed on the general purpose digital computers.

The remainder of the paper is organized as follows. Section 2 states the localization problem and introduces the robust model transformation formulation. Section 3 reviews the classical LPNN framework and defines the neural dynamics of the presented PNN, whose stability and convergence properties are then briefly discussed in Section 4. To ensure a fair comparison between the proposed neurodynamic method and the state-of-the-art convex optimization counterparts in terms of computational expense, its algorithmic complexity when implementing in a numerical fashion is also analyzed in Section 4. Section 5 evaluates the performance of our approach through computer simulations. Finally, conclusions are drawn in Section 6.

2. Problem formulation

Consider a TDOA-based localization system in k -dimensional space ($k = 2$ or 3) with $L \geq k+1$ sensors and a single source. The known sensor positions and unknown source location are denoted by $\mathbf{x}_i \in \mathbb{R}^k$ (for $i = 1, 2, \dots, L$) and $\mathbf{x} \in \mathbb{R}^k$, respectively. As demonstrated in Fig. 1, the local clocks of the sensors are well synchronized such that the received signal timestamp t_i (for $i = 1, 2, \dots, L$) can be collected from the i th sensor, whereas the time at which the signal is emitted from the source, t_0 , is unknown because there is no synchronization between the source and sensors. Without loss of generality, the first sensor is designated

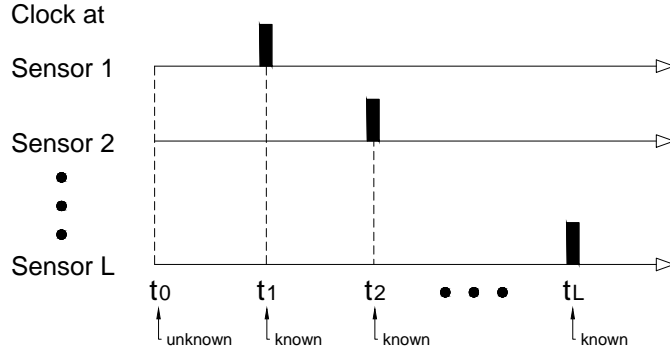


Fig. 1. Signal timestamp diagram of TDOA-based localization system.

as the reference and the TDOA measurements are modeled as

$$t_{i,1} = \frac{1}{c}(\|\mathbf{x} - \mathbf{x}_i\|_2 - \|\mathbf{x} - \mathbf{x}_1\|_2 + n_{i,1} + b_{i,1}) = t_i - t_1, \quad i = 2, 3, \dots, L, \quad (1)$$

where c denotes the signal propagation speed, $\|\cdot\|_2$ represents the ℓ_2 -norm of a vector, $n_{i,1} = n_i - n_1$ and $b_{i,1} = q_i - q_1$ (both for $i = 2, 3, \dots, L$) are the measurement noise and possible NLOS error in the corresponding range difference measurement, respectively, n_i (for $i = 1, 2, \dots, L$) is assumed to be zero-mean Gaussian noise with variance σ_i^2 , and q_i (for $i = 1, 2, \dots, L$) equals either 0 or a positive bias error e_i , contingent on whether the path between the i th sensor and source is line-of-sight (LOS) or NLOS. Before proceeding with the formulation derivation, we decompose the TDOA measurements in (1) into the related TOA components

$$t_i - t_0 = \frac{1}{c}(\|\mathbf{x} - \mathbf{x}_i\|_2 + n_i + q_i), \quad i = 1, 2, \dots, L \quad (2)$$

by making as if the synchronization between the source and sensors is established, namely, including t_0 as a variable of interest.

Exhibiting less sensitivity to outliers than the conventional ℓ_2 -norm criterion, the ℓ_1 -norm has been widely utilized in robust signal processing, with low-rank matrix completion under impulsive noise circumstances [35], robust principal component analysis [36], and sensor network localization under Laplacian noise assumption [37] being a few representative applications of it. Borrowing the

similar idea, we employ the LAD cost function as the objective of minimization to mitigate the positive bias errors in (2):

$$\min_{t_0, \mathbf{x}} \sum_{i=1}^L |(t_i - t_0)c - \|\mathbf{x} - \mathbf{x}_i\|_2|.$$

To bind the nuisance variable t_0 , the temporal constraints¹

$$0 \leq t_0 \leq t_i, \quad i = 1, 2, \dots, L, \quad (3)$$

geometrical constraints by the triangle inequalities [38]

$$(t_i - t_0)c + (t_j - t_0)c \geq \|\mathbf{x}_i - \mathbf{x}_j\|_2, \quad i \neq j, \quad i, j = 1, 2, \dots, L, \quad (4)$$

and general consensus that e_i is much greater than $|n_i|$ are thereupon incorporated into the formulation, yielding:

$$\min_{t_0, \mathbf{x}, \mathbf{d}} \sum_{i=1}^L |(t_i - t_0)c - d_i|$$

$$\text{s.t. } d_i^2 = \|\mathbf{x} - \mathbf{x}_i\|_2^2, \quad i = 1, 2, \dots, L, \quad (5a)$$

$$d_i \geq 0, \quad i = 1, 2, \dots, L, \quad (5b)$$

$$(3), (4),$$

$$(t_i - t_0)c \geq d_i, \quad i = 1, 2, \dots, L, \quad (5c)$$

where $\mathbf{d} = [d_1, d_2, \dots, d_L]^T \in \mathbb{R}^L$ is a vector containing the auxiliary variables for source-sensor distances, and the constraint $d_i = \|\mathbf{x} - \mathbf{x}_i\|_2$ (for $i = 1, 2, \dots, L$) is replaced by (5a) and (5b) in the quadratic form to avoid ill-posing [31]. Falling into the category of nonlinear and nonconvex constrained optimization problems, (5) is appropriately tackled in the next section by constructing a dynamical system whose equilibrium state is reached at a Karush-Kuhn-Tucker (KKT) point of the underlying problem.

¹The temporal constraints are premised on $t_i > 0$ so as to be meaningful.

3. Preliminaries and proposed neurodynamic method

Assume that we have a nonlinear programming problem with equality constraints:

$$\min_{\mathbf{z}} f(\mathbf{z}), \quad \text{s.t. } \mathbf{h}(\mathbf{z}) = \mathbf{0}_M, \quad (6)$$

where $\mathbf{z} \in \mathbb{R}^N$, $f: \mathbb{R}^N \rightarrow \mathbb{R}$, $\mathbf{h}(\mathbf{z}) = [h_1(\mathbf{z}), h_2(\mathbf{z}), \dots, h_M(\mathbf{z})]^T \in \mathbb{R}^M$ is an M -dimensional vector-valued function of N variables with $M \leq N$, the functions $f(\mathbf{z})$ and $h_i(\mathbf{z})$ (for $i = 1, 2, \dots, M$) are supposed to be twice differentiable, and $\mathbf{0}_M \in \mathbb{R}^M$ denotes an all-zero vector of length M . In a nutshell, the widely used LPNN approach [24] deals with (6) by invoking the Lagrange multiplier theory and designing a neurodynamic model whose time-domain transient behavior is defined as

$$\frac{d\mathbf{z}}{dt} = -\nabla_{\mathbf{z}} \mathcal{L}_*(\mathbf{z}, \boldsymbol{\lambda}), \quad (7a)$$

$$\frac{d\boldsymbol{\lambda}}{dt} = \nabla_{\boldsymbol{\lambda}} \mathcal{L}_*(\mathbf{z}, \boldsymbol{\lambda}), \quad (7b)$$

where $\nabla_{\mathbf{z}}(\cdot) \in \mathbb{R}^N$ denotes the gradient of a function at \mathbf{z} , $\boldsymbol{\lambda} \in \mathbb{R}^M$ is a vector containing the Lagrange multipliers for the constraints in (6), \mathbf{z} and $\boldsymbol{\lambda}$ are assigned physical meanings as the activities of the variable and Lagrangian neurons, respectively, and $\mathcal{L}_*(\mathbf{z}, \boldsymbol{\lambda})$ can be either the Lagrangian or augmented Lagrangian of (6), differing in the stability of the built system under nonconvexity. In the dynamic process of the LPNN, (7a) ensures that the value of $\mathcal{L}_*(\mathbf{z}, \boldsymbol{\lambda})$ decreases over time, whereas (7b) plays a role in leading the solution into the feasible region. After performing appropriate initialization of the variable and Lagrangian neurons, the network governed by (7) is expected to approach an equilibrium point satisfying the first-order necessary conditions of optimality (a.k.a. the KKT conditions).

It is obvious that (5) does not conform to the paradigm shown in (6) owing to the existence of numerous inequality constraints. Instead of introducing slack variables [31, 33] to fit in with (6), in the following we seek for a simpler way to

directly handle the general constrained optimization problem (GCOP)

$$\min_{\mathbf{z}} f(\mathbf{z}), \quad \text{s.t. } \mathbf{g}(\mathbf{z}) \leq \mathbf{0}_K, \quad \mathbf{h}(\mathbf{z}) = \mathbf{0}_M, \quad (8)$$

where the definitions pertaining to \mathbf{z} , $\boldsymbol{\lambda}$, f , and \mathbf{h} remain the same as those in (6) except that $M \leq N$ is no longer requested, the K -dimensional vector-valued function $\mathbf{g}(\mathbf{z}) = [g_1(\mathbf{z}), g_2(\mathbf{z}), \dots, g_K(\mathbf{z})]^T \in \mathbb{R}^K$ is assumed to be twice differentiable, and the vector inequality $\mathbf{a} \leq \mathbf{b}$ means each component of \mathbf{a} is less than or equal to each corresponding component of \mathbf{b} .

The Lagrangian of (8) is $\mathcal{L}(\mathbf{z}, \boldsymbol{\nu}) = f(\mathbf{z}) + \boldsymbol{\mu}^T \mathbf{g}(\mathbf{z}) + \boldsymbol{\lambda}^T \mathbf{h}(\mathbf{z})$. Here, we have $\boldsymbol{\nu} = [\boldsymbol{\mu}^T, \boldsymbol{\lambda}^T]^T \in \mathbb{R}^{K+M}$, where $\boldsymbol{\mu} = [\mu_1, \mu_2, \dots, \mu_K]^T \in \mathbb{R}^K$ and $\boldsymbol{\lambda} = [\lambda_1, \lambda_2, \dots, \lambda_M]^T \in \mathbb{R}^M$ are the vectors containing Lagrange multipliers for the inequality and equality constraints in (8), respectively. The KKT conditions [42] for (8) that a pair $(\mathbf{z}^*, \boldsymbol{\nu}^*)$ satisfies², namely, the first-order necessary conditions for \mathbf{z}^* to be a local minimizer of (8), are

$$\begin{cases} \nabla_{\mathbf{z}} \mathcal{L}(\mathbf{z}^*, \boldsymbol{\nu}^*) = \mathbf{0}_N, & (9a) \\ g_i(\mathbf{z}^*) \leq 0, \mu_i^* \geq 0, \mu_i^* g_i(\mathbf{z}^*) = 0, \quad i = 1, 2, \dots, K, & (9b) \\ \mathbf{h}(\mathbf{z}^*) = \mathbf{0}_M. & (9c) \end{cases}$$

Analogous to the strategy taken by [28], we point out that the KKT conditions in (9) actually share the same solution set with

$$\begin{cases} \nabla_{\mathbf{z}} \mathcal{L}_\rho(\mathbf{z}^*, \boldsymbol{\nu}^*) = \mathbf{0}_N, & (10a) \\ [\mu_i^* + \alpha g_i(\mathbf{z}^*)]^+ = \mu_i^*, \quad i = 1, 2, \dots, K, & (10b) \\ \mathbf{h}(\mathbf{z}^*) = \mathbf{0}_M, & (10c) \end{cases}$$

where $\mathcal{L}_\rho(\mathbf{z}, \boldsymbol{\nu}) = \mathcal{L}(\mathbf{z}, \boldsymbol{\nu}) + \frac{\rho}{2} \left\{ \sum_{i=1}^K [\mu_i g_i(\mathbf{z})]^2 + \sum_{i=1}^M [\lambda_i h_i(\mathbf{z})]^2 \right\}$ is a redefined augmented Lagrangian of (8), the scale factor $\alpha > 0$ indicates the convergence rate of the neural network and we let $\alpha = 1$ in this paper for simplicity, $\rho > 0$ is the augmented Lagrangian parameter, and the operator

$$[\cdot]^+ = \max(\cdot, 0) \quad (11)$$

²In this paper, we stipulate that the asterisk in the superscript of a vector is by default applied to each component of the vector.

is introduced to re-express the primal feasibility, dual feasibility, and complementarity conditions for the inequality constraints in a projection form. The equivalence between the solution sets of (9) and (10) is illustrated in the proposition below.

Proposition 1. Denote the solution sets of equations in (9) and (10) by Ω_1 and Ω_2 , respectively, then $\Omega_1 = \Omega_2$.

Proof. We begin with proving that (9b) is true if and only if (10b) is true.

Sufficiency:

The conditions in (9b) are partitioned into two cases as: (i) $g_i(\mathbf{z}^*) = 0, \mu_i^* \geq 0$, and (ii) $g_i(\mathbf{z}^*) < 0, \mu_i^* = 0$. The equalities in (10b) can be trivially deduced in both two cases, thus the sufficiency holds.

Necessity:

Case 1: $\mu_i^* + \alpha g_i(\mathbf{z}^*) \geq 0$.

It follows from (10b) and (11) that $[\mu_i^* + \alpha g_i(\mathbf{z}^*)]^+ = \mu_i^* + \alpha g_i(\mathbf{z}^*) = \mu_i^*$, which subsequently implies $g_i(\mathbf{z}^*) = 0$ and $\mu_i^* \geq 0$.

Case 2: $\mu_i^* + \alpha g_i(\mathbf{z}^*) < 0$.

Likewise, we arrive at $[\mu_i^* + \alpha g_i(\mathbf{z}^*)]^+ = 0 = \mu_i^*$ and $g_i(\mathbf{z}^*) < 0$.

It is evident that the conditions in (9b) are formed by merging the two cases together. Therefore, the necessity is satisfied.

In this way, we now only need to prove that (9a) and (10a) are equivalent to each other under the conditions in (9b) and (9c). The gradient of $\mathcal{L}_\rho(\mathbf{z}, \boldsymbol{\nu})$ at \mathbf{z} is calculated as

$$\nabla_{\mathbf{z}} \mathcal{L}_\rho(\mathbf{z}, \boldsymbol{\nu}) = \nabla_{\mathbf{z}} \mathcal{L}(\mathbf{z}, \boldsymbol{\nu}) + \rho \left[\sum_{i=1}^K \mu_i^2 g_i(\mathbf{z}) \nabla_{\mathbf{z}} g_i(\mathbf{z}) + \sum_{i=1}^M \lambda_i^2 h_i(\mathbf{z}) \nabla_{\mathbf{z}} h_i(\mathbf{z}) \right]. \quad (12)$$

Substituting the conditions in (9b) and (9c) into (12) at $(\mathbf{z}^*, \boldsymbol{\nu}^*)$ produces $\nabla_{\mathbf{z}} \mathcal{L}_\rho(\mathbf{z}^*, \boldsymbol{\nu}^*) = \nabla_{\mathbf{z}} \mathcal{L}(\mathbf{z}^*, \boldsymbol{\nu}^*)$, which verifies the equivalence between (9a) and (10a). The proof is complete.

Based on (10), a KKT point of the GCOP (8) is to be searched by employing

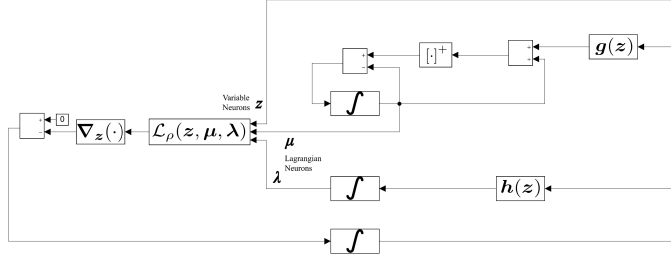


Fig. 2. Sketch for neural network defined by (13).

a three-layer PNN, with its dynamical equations being given by

$$\frac{dz}{dt} = -\nabla_{\mathbf{z}} \mathcal{L}_{\rho}(\mathbf{z}, \boldsymbol{\nu}), \quad (13a)$$

$$\frac{d\mu_i}{dt} = -\mu_i + [\mu_i + g_i(\mathbf{z})]^+, \quad i = 1, 2, \dots, K, \quad (13b)$$

$$\frac{d\boldsymbol{\lambda}}{dt} = \mathbf{h}(\mathbf{z}). \quad (13c)$$

A simplified block diagram of how such a neural network can be implemented on hardware is sketched in Fig. 2. What may be noteworthy is that (13) can be viewed as either a projection-type extension of the standard LPNN [24], a GCOP-treatable augmentation of the neurodynamic model in [28], or a simplification leaving out the bound constraints of that in [41]. On this account, several existing analyses in the literature will be referenced for the property discussion on (13) in the related sections.

In what follows, the neurodynamic system described by (13) is exploited for working out the solution to (5). To meet the higher-order (more precisely, twice in our scenario) differentiability condition for the neural network implementation [24, 41], the absolute value function in (5) is replaced by the following smoothed robust loss function with arbitrary-order derivatives³ [44]:

$$f_1(z) = \frac{\ln((e^{\gamma z} + e^{-\gamma z})/2)}{\gamma},$$

³Note that the celebrated Huber loss function which is a trade-off between the ℓ_1 - and ℓ_2 -norm [43] also suffers from the differentiability issues, i.e., it is only first-order differentiable [40].

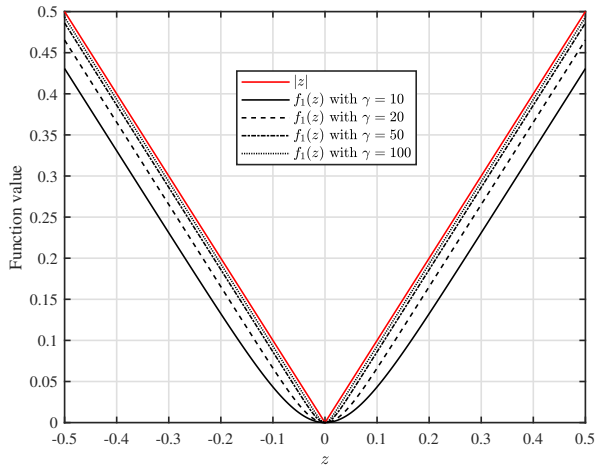


Fig. 3. Comparison of the functions $|z|$ and $f(z)$.

where $\gamma > 0$ is a predefined parameter and $\log(\cdot)$ denotes the logarithm operation with base e . For illustrative purpose, the comparison between the absolute value function $|z|$ and $f_1(z)$ is provided in Fig. 3, from which it is clearly seen that acceptable approximation can be achieved if a sufficiently large γ is chosen. Accordingly, the problem (5) is approximated by

$$\min_{t_0, \mathbf{x}, \mathbf{d}} \sum_{i=1}^L f_1((t_i - t_0)c - d_i), \quad \text{s.t. (3), (4), (5a)–(5c),}$$

which can then be cast into the standard GCOP form shown in (8) by letting

$$\mathbf{z} = [t_0, \mathbf{x}^T, \mathbf{d}^T]^T \in \mathbb{R}^{L+k+1},$$

$$N = L + k + 1,$$

$$K = \frac{L^2 + 5L + 2}{2},$$

$$M = L,$$

$$f(\mathbf{z}) = \sum_{i=1}^L f_1((t_i - t_0)c - d_i),$$

$$g_1(\mathbf{z}) = -t_0,$$

$$g_{i+1}(\mathbf{z}) = t_0 - t_i, \quad i = 1, 2, \dots, L,$$

$$\begin{aligned}
g_{i+L+1}(\mathbf{z}) &= -d_i, \quad i = 1, 2, \dots, L, \\
g_{i+2L+1}(\mathbf{z}) &= d_i - (t_i - t_0)c, \quad i = 1, 2, \dots, L, \\
[\mathbf{g}(\mathbf{z})]_{3L+2:K} &= \left[g_{3L+2}(\mathbf{z}), \dots, g_{\frac{(2L-i)(i-1)}{2}+j-i+3L+1}(\mathbf{z}), \dots, g_K(\mathbf{z}) \right]^T \\
&= [g_{1,2}(\mathbf{z}), \dots, g_{1,L}(\mathbf{z}), g_{2,3}(\mathbf{z}), \dots, g_{L-1,L}(\mathbf{z})]^T \in \mathbb{R}^{\frac{L(L-1)}{2}} \\
h_i(\mathbf{z}) &= d_i^2 - \|\mathbf{x} - \mathbf{x}_i\|_2^2, \quad i = 1, 2, \dots, L,
\end{aligned}$$

where

$$g_{i,j}(\mathbf{z}) = (2t_0 - t_i - t_j)c + \|\mathbf{x}_i - \mathbf{x}_j\|_2, \quad i = 1, 2, \dots, L-1, \quad j = i+1, i+2, \dots, L.$$

While the dynamical equations are readily constructed pursuant to the rules in (13), a more detailed description of the most crucial step (13a) is presented as follows:

$$\begin{aligned}
\frac{d\mathbf{z}}{dt} &= \left[\frac{dt_0}{dt}, \left(\frac{d\mathbf{x}}{dt} \right)^T, \left(\frac{d\mathbf{d}}{dt} \right)^T \right]^T = -\nabla_{\mathbf{z}} \mathcal{L}_\rho(\mathbf{z}, \boldsymbol{\nu}) = -\frac{\partial \mathcal{L}_\rho(\mathbf{z}, \boldsymbol{\nu})}{\partial \mathbf{z}} \\
&= -\left[\frac{\partial \mathcal{L}_\rho(\mathbf{z}, \boldsymbol{\nu})}{\partial t_0}, \left(\frac{\partial \mathcal{L}_\rho(\mathbf{z}, \boldsymbol{\nu})}{\partial \mathbf{x}} \right)^T, \left(\frac{\partial \mathcal{L}_\rho(\mathbf{z}, \boldsymbol{\nu})}{\partial \mathbf{d}} \right)^T \right]^T,
\end{aligned}$$

where

$$\begin{aligned}
\frac{\partial \mathcal{L}_\rho(\mathbf{z}, \boldsymbol{\nu})}{\partial t_0} &= c \sum_{i=1}^L \frac{e^{2\gamma[d_i+(t_0-t_i)c]} - 1}{e^{2\gamma[d_i+(t_0-t_i)c]} + 1} - \mu_1 + \sum_{i=1}^L \mu_{i+1} + c \sum_{i=1}^L \mu_{i+2L+1} \\
&+ 2c \sum_{i=1}^{L-1} \sum_{j=i+1}^L \mu_{\frac{(2L-i)(i-1)}{2}+j-i+3L+1} + \rho \left\{ \mu_1^2 t_0 + \sum_{i=1}^L \mu_{i+1}^2 (t_0 - t_i) \right. \\
&+ c \sum_{i=1}^L \mu_{i+2L+1}^2 [d_i - (t_i - t_0)c] + 2c \sum_{i=1}^{L-1} \sum_{j=i+1}^L \mu_{\frac{(2L-i)(i-1)}{2}+j-i+3L+1}^2 \\
&\left. [(2t_0 - t_i - t_j)c + \|\mathbf{x}_i - \mathbf{x}_j\|_2] \right\}, \\
\frac{\partial \mathcal{L}_\rho(\mathbf{z}, \boldsymbol{\nu})}{\partial \mathbf{x}} &= 2 \sum_{i=1}^L \left[\lambda_i + \rho \lambda_i^2 \left(d_i^2 - \|\mathbf{x} - \mathbf{x}_i\|_2^2 \right) \right] (\mathbf{x}_i - \mathbf{x}), \\
\frac{\partial \mathcal{L}_\rho(\mathbf{z}, \boldsymbol{\nu})}{\partial \mathbf{d}} &= \left[\frac{\partial \mathcal{L}_\rho(\mathbf{z}, \boldsymbol{\nu})}{\partial d_1}, \frac{\partial \mathcal{L}_\rho(\mathbf{z}, \boldsymbol{\nu})}{\partial d_2}, \dots, \frac{\partial \mathcal{L}_\rho(\mathbf{z}, \boldsymbol{\nu})}{\partial d_L} \right]^T,
\end{aligned}$$

and

$$\begin{aligned} \frac{\partial \mathcal{L}_\rho(\mathbf{z}, \boldsymbol{\nu})}{\partial d_i} &= \frac{e^{2\gamma[d_i+(t_0-t_i)c]} - 1}{e^{2\gamma[d_i+(t_0-t_i)c]} + 1} - \mu_{i+L+1} + \mu_{i+2L+1} + 2\lambda_i d_i + \rho \left\{ \mu_{i+L+1}^2 d_i \right. \\ &\quad \left. + \mu_{i+2L+1}^2 [d_i - (t_i - t_0)c] + 2\lambda_i^2 d_i \left(d_i^2 - \|\mathbf{x} - \mathbf{x}_i\|_2^2 \right) \right\}, \quad i = 1, 2, \dots, L. \end{aligned}$$

4. Stability, convergence, and complexity analyses

Since the original objective function of our formulation lies in the ℓ_1 -space, we succinctly term the proposed projection-type recurrent neural network method ℓ_1 -PNN. In this section, several important aspects including the stability, convergence, and complexity properties of ℓ_1 -PNN are discussed.

4.1. Local stability and convergence analysis

As a preparation for the formal statements and by taking the GCOP (8) as an example, we define three concepts which frequently appear in the optimization literature:

Definition 1. (**Feasible region**). A feasible region is the set of all possible solutions to an optimization problem (namely, the GCOP (8)) that satisfy the problem's constraints ($\mathbf{g}(\tilde{\mathbf{z}}) \leq \mathbf{0}_K$ and $\mathbf{h}(\tilde{\mathbf{z}}) = \mathbf{0}_M$).

Definition 2. (**Regularity condition**). A feasible point $\tilde{\mathbf{z}}$ is said to be a regular point if the gradients of the active inequality constraints (i.e., $\nabla_{\mathbf{z}} g_i(\tilde{\mathbf{z}}), \forall i \in \mathcal{I} = \{i | g_i(\tilde{\mathbf{z}}) = 0\}$) and those of the equality constraints (i.e., $\nabla_{\mathbf{z}} h_i(\tilde{\mathbf{z}})$ for $i = 1, 2, \dots, M$) are linearly independent at $\tilde{\mathbf{z}}$. This is a.k.a. the linear independence constraint qualification (LICQ).

Definition 3. (**Strict local minimum**). A point \mathbf{z}^* is said to be a strict local minimum if $f(\mathbf{z}^*) < f(\mathbf{z}), \forall \mathbf{z} \in \mathcal{N}(\mathbf{z}^*, \delta) \cap \mathbf{S}$, where $\mathcal{N}(\mathbf{z}^*, \delta)$ represents the neighborhood of the point \mathbf{z}^* with radius $\delta > 0$ and \mathbf{S} denotes the feasible region.

A lemma presenting the second-order sufficient conditions (SOSC) [45] is then introduced as:

Lemma 1. (SOSC [45]). Let \mathbf{z}^* be a feasible and regular point of the GCOP (8). If there exists a $\boldsymbol{\nu}^* = [\boldsymbol{\mu}^{*T}, \boldsymbol{\lambda}^{*T}]^T \in \mathbb{R}^{K+M}$, such that $(\mathbf{z}^*, \boldsymbol{\nu}^*)$ is a KKT

pair and $\nabla_{\mathbf{z}\mathbf{z}}^2 \bar{\mathcal{L}}(\mathbf{z}^*, \boldsymbol{\nu}^*)$ is positive definite on the cone

$$\mathcal{C} = \left\{ \mathbf{y} \in \mathbb{R}^N \mid \begin{aligned} & [\nabla_{\mathbf{z}} g_i(\mathbf{z}^*)]^T \mathbf{y} = 0, \forall i \in \mathcal{I}_+, \quad [\nabla_{\mathbf{z}} g_i(\mathbf{z}^*)]^T \mathbf{y} \leq 0, \forall i \in \mathcal{I}_0, \\ & [\nabla_{\mathbf{z}} h_i(\mathbf{z}^*)]^T \mathbf{y} = 0, \forall i = 1, 2, \dots, M, \quad \mathbf{y} \neq \mathbf{0}_N \end{aligned} \right\},$$

where $\bar{\mathcal{L}}(\mathbf{z}^*, \boldsymbol{\nu}^*) = f(\mathbf{z}^*) + \sum_{i \in \mathcal{I}} \mu_i^* g_i(\mathbf{z}^*) + \sum_{i=1}^M \lambda_i^* h_i(\mathbf{z}^*)$ is the restricted Lagrangian function at $(\mathbf{z}^*, \boldsymbol{\nu}^*)$, and $\mathcal{I}_+ = \{i \in \mathcal{I} \mid \mu_i^* > 0\}$ and $\mathcal{I}_0 = \{i \in \mathcal{I} \mid \mu_i^* = 0\}$ are often referred to as the sets of strongly active and weakly active constraints, respectively.

We now finally arrive at the following lemma in which the analytical results concerning the behaviors of iterative sequences produced by (13) are established.

Lemma 2. (Local stability [41]). Suppose that $(\mathbf{z}^*, \boldsymbol{\nu}^*)$ is a KKT point of the GCOP (8) satisfying the SOSC in Lemma 1. There exists a sufficiently large $\rho > 0$, such that the neurodynamic system described by (13) is asymptotically stable at $(\mathbf{z}^*, \boldsymbol{\nu}^*)$, where \mathbf{z}^* is a strict local minimum of the GCOP (8).

The detailed proof of Lemma 2 is omitted, because it constitutes a special case of the analysis of Theorem 2 in [41] if we set the lower and upper bounds therein as negative and positive infinities, respectively. Based on Lemma 2, we embark on a careful examination of the local stability of ℓ_1 -PNN below. In general, the source onset time should be a proper value at least greater than 0 [20], the positions of the sensors are different from that of the source (otherwise there is no need for localization), and the positive bias error is much larger than the magnitude of the measurement noise in a TOA measurement under NLOS conditions [13]. Therefore, the inequality constraints in (5) are actually all inactive (viz. $\mathcal{I} = \emptyset$), which means that the LICQ in our case is subject to only the equality constraints. The gradients of the equality constraints in (5) at a KKT point $(\mathbf{z}^*, \boldsymbol{\nu}^*)$ are calculated as

$$\begin{aligned} \nabla_{\mathbf{z}} \mathbf{h}(\mathbf{z}^*) &= \left. \frac{\partial \mathbf{h}(\mathbf{z})}{\partial \mathbf{z}} \right|_{\mathbf{z}=\mathbf{z}^*} = \left[\frac{\partial h_1(\mathbf{z}^*)}{\partial \mathbf{z}}, \frac{\partial h_2(\mathbf{z}^*)}{\partial \mathbf{z}}, \dots, \frac{\partial h_L(\mathbf{z}^*)}{\partial \mathbf{z}} \right]^T \\ &= \left[\mathbf{0}_L \mid 2 \left(\mathbf{X}^T - \mathbf{1}_L \mathbf{x}^{*T} \right) \mid 2 \text{diag}(\mathbf{d}^*) \right], \end{aligned} \quad (18)$$

where $\mathbf{1}_L \in \mathbb{R}^L$ is an all-one vector of length L , $\text{diag}(\mathbf{a})$ stands for a diagonal matrix with vector \mathbf{a} being its main diagonal, and $\mathbf{X} = [\mathbf{x}_1, \mathbf{x}_2, \dots, \mathbf{x}_L] \in \mathbb{R}^{k \times L}$ represents a matrix including the positions of all sensors. Given the aforementioned practical considerations, we can easily deduce that the row vectors of the matrix in (18) are linearly independent and therewith $\mathcal{C} = \emptyset$. As a result, the SOS hold trivially, and from Lemma 2 our ℓ_1 -PNN is assured locally stable as long as the Lagrangian parameter takes a large enough value. It is worth mentioning that due to the nonconvexity of the problem being solved, we investigate only the local stability of ℓ_1 -PNN here, but refer the interested readers to [41, 46, 47] for the very recent developments of global convergence guaranteed neurodynamic optimization. Nevertheless, it is shown in Section 5 through extensive simulations that even local minimization can yield satisfactory performance in terms of positioning accuracy.

4.2. Complexity analysis

Since ℓ_1 -PNN is intended to be implemented analogously by designated hardware (e.g., application specific integrated circuits), it may not be meaningful to compare its complexity with those of the numerical approaches. Yet, we still manage to analyze the computational complexity of the neural network framework (13) when it is realized in a discrete and numerical manner [32]:

$$\begin{cases} \mathbf{z}_{(\kappa+1)} = \mathbf{z}_{(\kappa)} + \tau \frac{d\mathbf{z}}{dt}, \\ \boldsymbol{\mu}_{(\kappa+1)} = \boldsymbol{\mu}_{(\kappa)} + \tau \frac{d\boldsymbol{\mu}}{dt}, \\ \boldsymbol{\lambda}_{(\kappa+1)} = \boldsymbol{\lambda}_{(\kappa)} + \tau \frac{d\boldsymbol{\lambda}}{dt}, \end{cases} \quad (19)$$

where the subscript $(\cdot)_{(\kappa)}$ denotes the iteration index, τ is the step size, and the derivatives $\frac{d\mathbf{z}}{dt}$, $\frac{d\boldsymbol{\mu}}{dt}$, $\frac{d\boldsymbol{\lambda}}{dt}$ follow the definitions in (13). With the help of Horner's scheme [48], the evaluation of a polynomial of degree n with fixed-size coefficients can be computed in $\mathcal{O}(n)$ time. Then, by considering polynomial evaluation as the operation in each step of (19) governing the computational complexity, it is not hard to conclude that the dominant complexity of ℓ_1 -PNN is

Table 1: Complexity of considered NLOS mitigation algorithms

Algorithm	Complexity
ℓ_1 -PNN	$\mathcal{O}(N_{\text{PNN}}L^2)$
SDP-Robust-Refinement-1	$\mathcal{O}(L^{6.5})$
SDP-Robust-Refinement-2	$\mathcal{O}(L^{6.5})$
SDP-TOA	$\mathcal{O}(L^4)$

$\mathcal{O}\left(N_{\text{PNN}}\left(\max(\zeta, 3)+5k+L\max(\zeta, 5)+\frac{L^2+5L+2}{2}+2L\right)\right) = \mathcal{O}(N_{\text{PNN}}L^2)$, where ζ is the degree of the Maclaurin polynomial for the hyperbolic tangent function $\frac{e^{2\gamma[d_i+(t_0-t_i)c]}-1}{e^{2\gamma[d_i+(t_0-t_i)c]}+1}$ and N_{PNN} is the iteration number of the PNN using discrete realization. Table 1 presents a comparison of complexity of the proposed neurodynamic method for solving (5) (termed ℓ_1 -PNN), SDP-based robust method for solving Formulation 1 in [19] (termed SDP-Robust-Refinement-1), SDP-based robust method for solving Formulation 2 in [19] (termed SDP-Robust-Refinement-2), and SDP-based model transformation method in [20] (termed SDP-TOA) as the function of L . Note that the naming of SDP-TOA is consistent with that in [19], and the computational costs of dealing with the mixed SDP/SOCP problems are determined by following the calculation rule in [49]. It can be concluded that ℓ_1 -PNN has a significantly lower complexity than those convex optimization approaches in [19, 20].

5. Simulation results

This section substantiates the efficacy of our proposed neurodynamic approach through simulation studies. To be specific, ℓ_1 -PNN is compared with representative NLOS mitigation algorithms including SDP-Robust-Refinement-1 in [19], SDP-Robust-Refinement-2 in [19], and SDP-TOA in [20] just as what have been provided in Table 1⁴, and additionally the separated constrained weighted LS (SCWLS) approach in [8]. Furthermore, the Cramér-Rao lower

⁴It is remarkable that the definition of matrix \mathbf{E} in [19] is incorrect and should be amended before putting the involved algorithms into use.

bounds (CRLBs) for positioning with TDOA measurements in the LOS [8] and NLOS [50] scenarios are also included as the benchmark (when applicable). It should be mentioned that the invocation of ℓ_1 -PNN and SDP-TOA needs only the sensor positions and known signal timestamps as the inputs, whereas additional prior knowledge of the error bound/noise variance is a must for SDP-Robust-Refinement-1, SDP-Robust-Refinement-2, and SCWLS. In the following numerical examples, a perfect upper bound of the NLOS error is always ensured and passed into SDP-Robust-Refinement-1 and SDP-Robust-Refinement-2. The CVX package [51] and MATLAB[®] ODE solver are utilized for realizing the convex programs and solving the systems of equations, respectively. All hyperparameters involved in SDP-TOA are assigned the same values as those in the demonstration program⁵ coded by the authors of [20]. As a global setup of ℓ_1 -PNN, the values held in the variable and Lagrangian neurons are initialized with 0s. For the selection of the augmented Lagrangian parameter ρ , the existing numerical results [41] demonstrate that a relatively large ρ can reduce transient oscillation of the neurodynamic model and speed up the convergence. In our simulations, we simply set $\rho = 5$ and it is observed that such a value always makes ℓ_1 -PNN settle down within several tens of time constants. Another predefined parameter associated with the quality of approximation to the original ℓ_1 -norm is fixed as $\gamma = 100$, based on which the resultant estimator is robust enough (see Fig. 3). All simulations are carried out using a laptop with Intel[®] Core[™] i7-10710U processor and 16 GB memory.

Basically, two representative configurations with $k = 2$ are covered. The first configuration considers source localization in a $20 \text{ m} \times 20 \text{ m}$ square region with $L = 8$ sensors being evenly placed on the perimeter of the area and a single source being deployed at $\mathbf{x} = [2, 3]^T \text{ m}$. On the other hand, a typical setting in [15] with multiple sensors and a single source, whose locations are all randomly selected from the $20 \text{ m} \times 20 \text{ m}$ square region in each Monte Carlo (MC) run, is adopted as the second configuration. The true value of the unknown source

⁵<https://github.com/xmuszq/Semidefinite-Programming-SDP-optimization>

onset time is fixed as $t_0 = 0.1$ s, while the known signal timestamps received at the sensors and the TDOA measurements in the simulated system are obtained in accordance with (2) and (1), respectively. Particularly, the signal propagation speed is set as $c = 1$ m/s to keep things simple, the zero-mean Gaussian distributed noise n_i is assumed to be of identical variance σ^2 for all i s, and the possible NLOS error in the TOA measurement between the source and i th sensor, namely q_i , is generated from the uniform distribution⁶ $\mathcal{U}(0, \omega_i)$.

In the first test, the dynamic behaviors of the estimated source position using ℓ_1 -PNN in the deterministic deployment scenario are investigated. Taking the LOS and a mild NLOS environments for instance, Fig. 4 plots the dynamics of the second and third variable neurons (i.e., those holding the variable \mathbf{x}) based on 100 MC runs. It is seen that ℓ_1 -PNN settles down and converges to a point close to the true source location within 20 to 40 time constants. For this reason, in the following we simply take the corresponding neuron output right after 40 time constants as the final position estimate produced by ℓ_1 -PNN. As a preliminary evaluation of ℓ_1 -PNN in comparison with other considered methods, Fig. 5 shows the empirical cumulative distribution function (CDF) of the Euclidean distance between source location and its estimate in the above-defined mild NLOS environment, from which we see that ℓ_1 -PNN and SDP-TOA demonstrate superior positioning performance. Next, the root mean square error (RMSE) criterion with 500 ensemble trials, defined as $\text{RMSE} = \sqrt{\frac{1}{500} \sum_{i=1}^{500} \|\hat{\mathbf{x}}^{\{i\}} - \mathbf{x}^{\{i\}}\|^2}$ where $\hat{\mathbf{x}}^{\{i\}}$ represents the estimate of source position in the i th MC run (namely $\mathbf{x}^{\{i\}}$), is utilized as a measure to further compare the location estimation performance of diverse approaches. Fig. 6 depicts the RMSE versus σ for the deterministic deployment scenario when the number of NLOS connections is fixed as $L_{\text{NLOS}} = 2$ and the parameter of uniform distribution is set to 5. Especially, comparison with the CRLB when no prior NLOS statistics are available (namely, the one depending only on LOS signals [50]) is also made. The results reveal that: (i) ℓ_1 -PNN exhibits the best robustness to NLOS propagation in

⁶Unquestionably, the corresponding source-sensor path is LOS if ω_i is assigned 0.

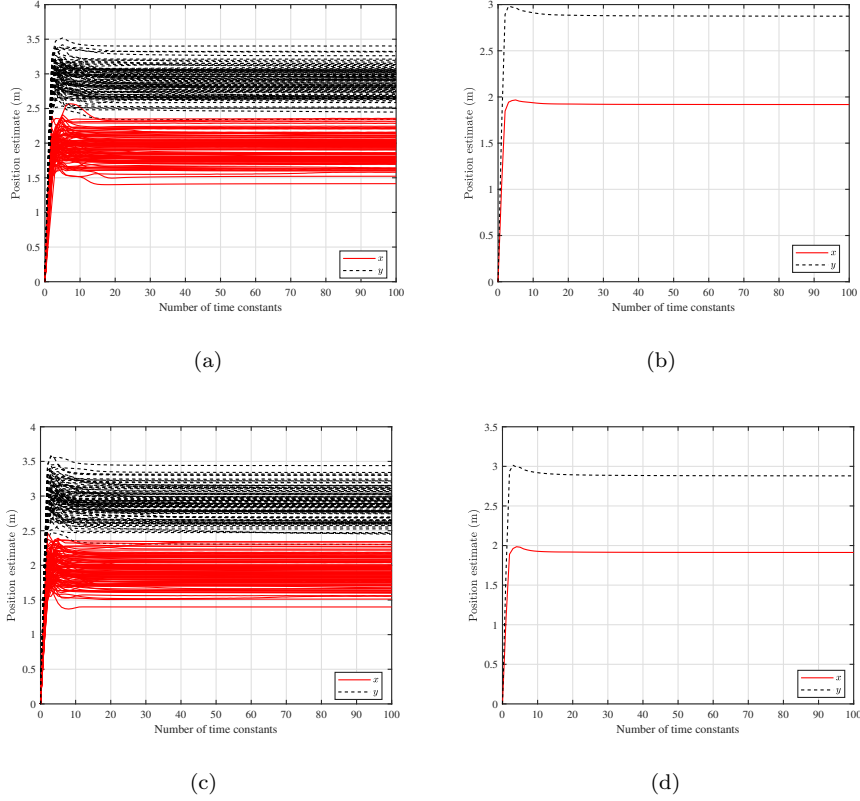


Fig. 4. Dynamic behaviors of estimated source position versus time constant number for deterministic deployment in LOS and mild NLOS environments. (a) Outputs of 100 independent trials when $\sigma^2 = 0.1$ and $\omega_i = 0$ for all is . (b) Mean of 100 outputs when $\sigma^2 = 0.1$ and $\omega_i = 0$ for all is . (c) Outputs of 100 independent trials when $\sigma^2 = 0.1$, $\omega_1 = 5$, $\omega_5 = 5$, and $\omega_i = 0$ for other is . (d) Mean of 100 outputs when $\sigma^2 = 0.1$, $\omega_1 = 5$, $\omega_5 = 5$, and $\omega_i = 0$ for other is .

such circumstances as long as σ is not large enough, and (ii) taking advantage of rather than simply discarding the NLOS links results in an improvement in performance.

The random deployment scenario with $L = 10$ is now considered to assess the localization performance of ℓ_1 -PNN together with other state-of-the-art algorithms under LOS and NLOS conditions. It must be pointed out that the

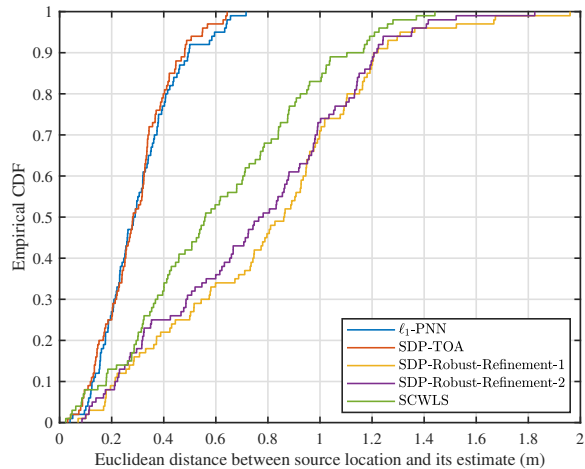


Fig. 5. Empirical CDF of Euclidean distance between source location and its estimate for deterministic deployment in mild NLOS environment based on 100 MC runs when $\sigma^2 = 0.1$, $\omega_1 = 5$, $\omega_5 = 5$, and $\omega_i = 0$ for other is .

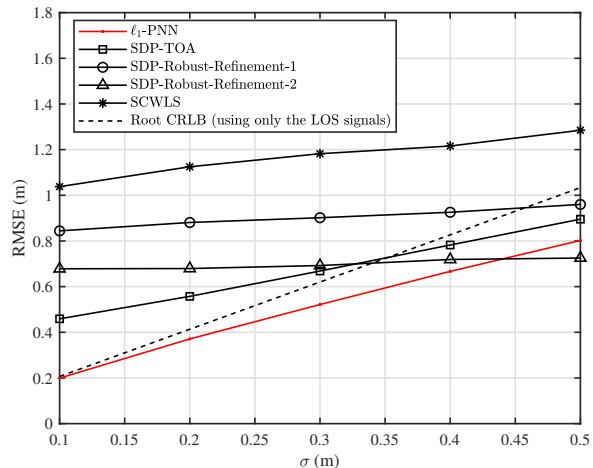


Fig. 6. RMSE versus σ for deterministic deployment in mild NLOS scenario when $\omega_1 = 5$, $\omega_2 = 5$ and $\omega_i = 0$ for other is .

setup is quite different from and in one sense more general than those in [17] and [19], as the sensors here are neither fixed nor placed on a certain circle but all randomly drawn from the square region. Fig. 7 illustrates the RMSE as a

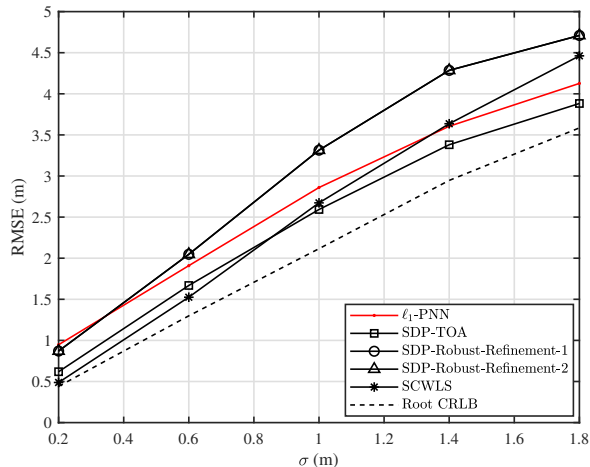
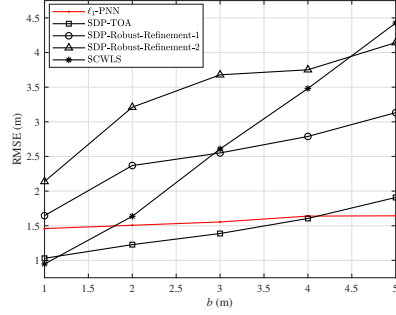
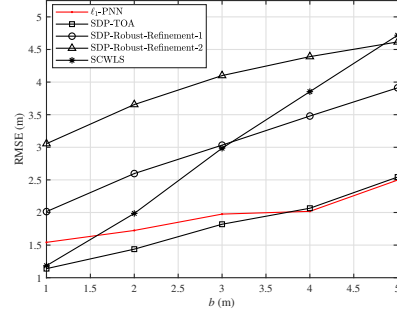


Fig. 7. RMSE versus σ in LOS scenario (viz. $L_{\text{NLOS}} = 0$).

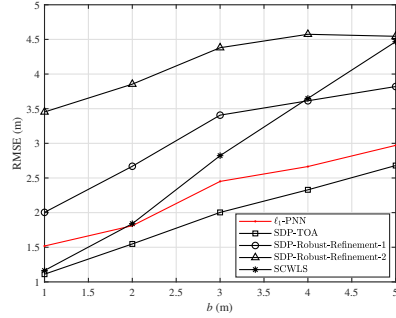
function of σ in the scenario where LOS transmissions are guaranteed for all source-sensor paths, i.e., $L_{\text{NLOS}} = 0$. Clearly, only the SCWLS algorithm at sufficiently lower-level measurement disturbances (e.g., when $\sigma = 0.2$ m) can attain the CRLB [8]. On the other side, there is always a performance gap between ℓ_1 -PNN and SDP-TOA/CRLB (i.e., SDP-TOA and CRLB are superior to ℓ_1 -PNN by about 0.25 m and 0.5 m across the whole range of σ). This is owing to the fact that SDP-TOA tightly approximates the ML estimator for small noise of the same level, whereas ℓ_1 -PNN derived in ℓ_1 -space is inherently suboptimal under the Gaussian noise assumption. It is also observed that the two worst-case robust methods SDP-Robust-Refinement-1 and SDP-Robust-Refinement-2 in general perform badly in the LOS scenario. We divide the test conditions in scenarios where NLOS propagation exists into two separate groups: (i) the path between the source and reference sensor is NLOS, and (ii) the path between the source and reference sensor is LOS. In each group, three diverse cases with $L_{\text{NLOS}} = 2, 5, 8$ are included, standing for the mild, moderate, and severe NLOS environments, respectively. Fig. 8 shows the comparison results with the detailed parameter settings being given in the caption. We can see that the location estimation accuracy of the non-robust SCWLS



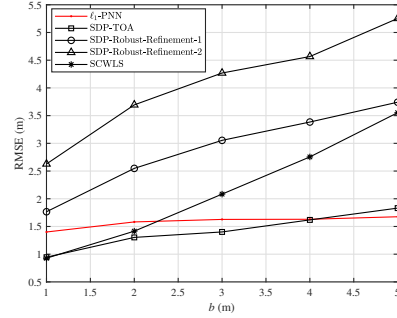
(a)



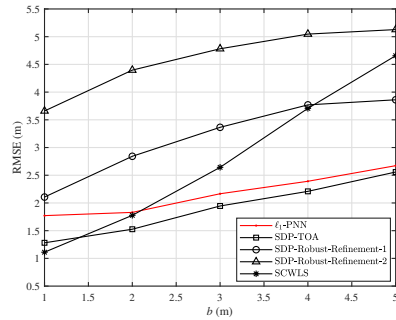
(b)



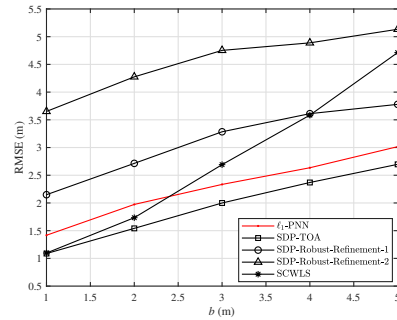
(c)



(d)



(e)



(f)

Fig. 8. RMSE versus parameter of uniform distribution b in different NLOS scenarios when $\sigma^2 = 0.1$. (a) $L_{\text{NLOS}} = 2$, $\omega_1 = b$. (b) $L_{\text{NLOS}} = 5$, $\omega_1 = b$. (c) $L_{\text{NLOS}} = 8$, $\omega_1 = b$. (d) $L_{\text{NLOS}} = 2$, $\omega_1 = 0$. (e) $L_{\text{NLOS}} = 5$, $\omega_1 = 0$. (f) $L_{\text{NLOS}} = 8$, $\omega_1 = 0$.

scheme deteriorates considerably as b increases. ℓ_1 -PNN and SDP-TOA have comparable RMSEs, and they both outperform SDP-Robust-Refinement-1 and SDP-Robust-Refinement-2. Note that although ℓ_1 -PNN is slightly inferior to SDP-TOA in most cases (e.g., for $b < 4$ in Figs. 8(a), 8(b), and 8(d) and all bs in Figs. 8(c), 8(e), and 8(f)), the former is computationally more efficient and gets rid of the cumbersome hyperparameter tuning problems.

6. Conclusion

In this paper, we proposed a robust model transformation formulation for TDOA-based source localization and devised a novel neurodynamic optimization solution to it. The new scheme does not require any *a priori* information except the positions of the sensors, received signal timestamps thereat, and signal propagation speed, as the mitigation of NLOS biases in the reconstructed TOA measurements are achieved via the ℓ_1 -norm criterion. To address the problem of non-differentiability of the ℓ_1 -norm, certain approximations were applied to the original objective function for yielding a differentiable surrogate. Benefiting from the use of a projection-type recurrent neural network approach, the biggest advantage of the presented algorithm over the existing ones is its quadratic computational complexity in L . Through the theoretical analysis and extensive simulation investigations, we verified that the dynamics of the proposed ℓ_1 -norm-based PNN are locally stable, and confirmed its superiority over several existing TDOA-based localization schemes in terms of the estimation accuracy.

Acknowledgment

This work was supported by the German Federal Ministry of Education and Research (BMBF) in the framework of the ASSIST ALL project under Grant FKZ:16SV8162.

The first author would also like to thank Ms Ge Cheng at China Railway Major Bridge Reconnaissance & Design Institute Co., Ltd. (BRDI), the team

of Telocate GmbH, and the Laboratory for Electrical Instrumentation of the University of Freiburg for their assistance with the manuscript preparation.

References

- [1] F. Höflinger, R. Zhang, J. Hoppe, A. Bannoura, L. M. Reindl, J. Wendeborg, M. Buhner, and C. Schindelhauer, “Acoustic self-calibrating system for indoor smartphone tracking (ASSIST),” in *Proc. 3rd. Int. Conf. Indoor Positioning and Indoor Navigation (IPIN)*, Sydney, Australia, Nov. 2012, pp. 1–9.
- [2] J. Bordoy, C. Schindelhauer, F. Höflinger, and L. M. Reindl, “Exploiting acoustic echoes for smartphone localization and microphone self-calibration,” *IEEE Trans. Instrum. Meas.*, vol. 69, no. 4, pp. 1484–1492, Apr. 2020.
- [3] V. G. Reju, A. W. H. Khong, and A. B. Sulaiman, “Localization of taps on solid surfaces for human-computer touch interfaces,” *IEEE Trans. Multimedia*, vol. 15, no. 6, pp. 1365–1376, Oct. 2013.
- [4] S. Li, L. D. Xu, and X. Wang, “Compressed sensing signal and data acquisition in wireless sensor networks and Internet of Things,” *IEEE Trans. Ind. Informat.*, vol. 9, no. 4, pp. 2177–2186, Nov. 2013.
- [5] Y. Huang, J. Benesty, G. Elko, and R. Mersereati, “Real-time passive source localization: A practical linear-correction least-squares approach,” *IEEE Trans. Speech Audio Process.*, vol. 9, no. 8, pp. 943–956, Nov. 2001.
- [6] N. Ono, H. Kohno, N. Ito, and S. Sagayama, “Blind alignment of asynchronously recorded signals for distributed microphone array,” in *Proc. IEEE Workshop Appl. Signal Process. Audio Acoustics*, New York, NY, USA, 2009, pp. 161–164.
- [7] N. Ono and S. Sagayama, “R-means localization: A simple iterative algorithm for range-difference-based source localization,” in *2010 IEEE Int.*

- Conf. Acoustics, Speech and Signal Process.*, Dallas, TX, USA, 2010, pp. 2718–2721.
- [8] L. Lin, H. C. So, F. K. W. Chan, Y. T. Chan, and K. C. Ho, “A new constrained weighted least squares algorithm for TDOA-based localization,” *Signal Process.*, vol. 93, no. 11, pp. 2872–2878, 2013.
- [9] H. C. So, “Source localization: Algorithms and analysis,” in *Handbook of Position Location: Theory, Practice and Advances*, S. A. Zekavat and M. Buehrer, Eds. New York, NY, USA: Wiley-IEEE Press, 2011.
- [10] I. Guvenc and C.-C. Chong, “A survey on TOA based wireless localization and NLOS mitigation techniques,” *IEEE Commun. Surveys Tuts.*, vol. 11, no. 3, pp. 107–124, Aug. 2009.
- [11] S. Tomic, M. Beko, R. Dinis, and P. Montezuma, “A robust bisection-based estimator for TOA-based target localization in NLOS environments,” *IEEE Commun. Lett.*, vol. 21, no. 11, pp. 2488–2491, Nov. 2017.
- [12] S. Tomic and M. Beko, “A bisection-based approach for exact target localization in NLOS environments,” *Signal Process.*, vol. 143, pp. 328–335, Feb. 2018.
- [13] G. Wang, H. Chen, Y. Li, and N. Ansari, “NLOS error mitigation for TOA-based localization via convex relaxation,” *IEEE Trans. Wireless Commun.*, vol. 13, no. 8, pp. 4119–4131, Aug. 2014.
- [14] H. Chen, G. Wang, and N. Ansari, “Improved robust TOA-based localization via NLOS balancing parameter estimation,” *IEEE Trans. Veh. Technol.*, vol. 68, no. 6, pp. 6177–6181, Jun. 2019.
- [15] W. Xiong and H. C. So, “TOA-based localization with NLOS mitigation via robust multidimensional similarity analysis,” *IEEE Signal Process. Lett.*, vol. 26, no. 9, pp. 1334–1338, Sep. 2019.

- [16] A. Prorok, L. Gonon, and A. Martinoli, “Online model estimation of ultra-wideband TDOA measurements for mobile robot localization,” *Proc. IEEE Int. Conf. Robot. Autom. (ICRA)*, Saint Paul, MN, May 2012, pp. 807–814.
- [17] G. Wang, A. M. C. So, and Y. Li, “Robust convex approximation methods for TDOA-based localization under NLOS conditions,” *IEEE Trans. Signal Process.*, vol. 64, no. 13, pp. 3281–3296, Jul. 2016.
- [18] W. Wang, G. Wang, F. Zhang, and Y. Li, “Second-order cone relaxation for TDOA-based localization under mixed LOS/NLOS conditions,” *IEEE Signal Process. Lett.*, vol. 23, no. 12, pp. 1872–1876, Dec. 2016.
- [19] G. Wang, W. Zhu and N. Ansari, “Robust TDOA-based localization for IoT via joint source position and NLOS error estimation,” *IEEE Internet Things J.*, vol. 6, no. 5, pp. 8529–8541, Oct. 2019.
- [20] Z. Su, G. Shao, and H. Liu, “Semidefinite programming for NLOS error mitigation in TDOA localization,” *IEEE Commun. Lett.*, vol. 22, no. 7, pp. 1430–1433, Jul. 2018.
- [21] W. Xiong, H. C. So, C. Schindelhauer, and J. Wendeberg, “Robust elliptic localization using worst-case formulation and convex approximation,” in *Proc. 16th IEEE Workshop Position., Navig., Commun. (WPNC)*, Bremen, Germany, Oct. 2019, pp. 1–6.
- [22] T. Le and K. C. Ho, “Uncovering source ranges from range differences observed by sensors at unknown positions: Fundamental theory,” *IEEE Trans. Signal Process.*, vol. 67, no. 10, pp. 2665–2678, May 2019.
- [23] E. Xu, Z. Ding, and S. Dasgupta, “Source localization in wireless sensor networks from signal time-of-arrival measurements,” *IEEE Trans. Signal Process.*, vol. 59, no. 6, pp. 2887–2897, Jun. 2011.
- [24] S. Zhang and A. G. Constantinides, “Lagrange programming neural networks,” *IEEE Trans. Circuits Syst. II: Anal. Digit. Signal Process.*, vol. 39, no. 7, pp. 441–452, Jul. 1992.

- [25] D. Tank and J. Hopfield, “Simple ‘neural’ optimization networks: An A/D converter, signal decision circuit, and a linear programming circuit,” *IEEE Trans. Circuits Syst.*, vol. 33, no. 5, pp. 533–541, May 1986.
- [26] M. P. Kennedy and L. O. Chua, “Neural networks for nonlinear programming,” *IEEE Trans. Circuits Syst.*, vol. 35, no. 5, pp. 554–562, May 1988.
- [27] A. Nazemi, “Solving general convex nonlinear optimization problems by an efficient neurodynamic model,” *Eng. Appl. Artif. Intell.*, vol. 26, no. 2, pp. 685–696, Feb. 2013.
- [28] X. Hu and J. Wang, “Convergence of a recurrent neural network for non-convex optimization based on an augmented Lagrangian function,” in *Proc. 4th Int. Symp. Neural Netw.*, Nanjing, China, Jun. 2007, pp. 194–203.
- [29] Z. Shi, H. Wang, C.-S. Leung, H. C. So, J. Liang, K.-F. Tsang, and A. G. Constantinides, Robust ellipse fitting based on Lagrange programming neural network and locally competitive algorithm, *Neurocomputing*, to be published, DOI: 10.1016/j.neucom.2020.02.100.
- [30] H. Wang, R. Feng, A. C. S. Leung, and K. F. Tsang, “Lagrange programming neural network approaches for robust time-of-arrival localization,” *Cogn. Comput.*, vol. 10, no. 1, pp. 23–34, Feb. 2018.
- [31] Z. Han, C. S. Leung, H. C. So, and A. G. Constantinides, “Augmented Lagrange programming neural network for localization using time-difference-of-arrival measurements,” *IEEE Trans. Neural Netw. Learn. Syst.*, vol. 29, no. 8, pp. 3879–3884, Aug. 2018.
- [32] J. Liang, C. S. Leung, and H. C. So, “Lagrange programming neural network approach for target localization in distributed MIMO radar,” *IEEE Trans. Signal Process.*, vol. 64, no. 6, pp. 1574–1585, Mar. 2016.
- [33] Z.-F. Han, C.-S. Leung, H. C. So, J. Sum, and A. G. Constantinides, “Non-line-of-sight mitigation via Lagrange programming neural networks

- in TOA-based localization,” in *Proc. Int. Conf. Neural Inf. Process.*, 2015, pp. 190–197.
- [34] C. Jia, D. Wang, J. Yin, X. Chen, and L. Zhang, “Joint multiple sources localization using TOA measurements based on Lagrange programming neural network,” *IEEE Access*, vol. 7, pp. 3247–3263, Dec. 2018.
- [35] A. Eriksson and A. van den Hengel, “Efficient computation of robust lowrank matrix approximations in the presence of missing data using the L_1 norm,” in *Proc. IEEE Conf. Comput. Vis. Pattern Recognit.*, San Francisco, CA, USA, Jun. 2010, pp. 771–778.
- [36] E. Candes, X. Li, Y. Ma, and J. Wright, “Robust principal component analysis?” *J. ACM*, vol. 58, no. 3, pp. 1–39, May 2011.
- [37] P. Oguz-Ekim, J. P. Gomes, J. Xavier, and P. Oliveira, “Robust localization of nodes and time-recursive tracking in sensor networks using noisy range measurements,” *IEEE Trans. Signal Process.*, vol. 59, no. 8, pp. 3930–3942, Aug. 2011.
- [38] O. Jean and A. J. Weiss, “Passive localization and synchronization using arbitrary signals,” *IEEE Trans. Signal Process.*, vol. 62, no. 8, pp. 2143–2150, Apr. 2014.
- [39] G. Lerman and T. Maunu, “An overview of robust subspace recovery,” *Proc. IEEE*, vol. 106, no. 8, pp. 1380–1410, Aug. 2018.
- [40] K. Fountoulakis and J. Gondzio, “A second-order method for strongly convex ℓ_1 -regularization problems,” *Math. Program.*, vol. 156, no. 12, pp. 189–219, 2016.
- [41] H. Che and J. Wang, “A collaborative neurodynamic approach to global and combinatorial optimization,” *Neural Netw.*, vol. 114, pp. 15–27, Jun. 2019.

- [42] J. Nocedal and S. J. Wright, *Numerical Optimization*, 2nd ed. New York, NY, USA: Springer, 2006.
- [43] R. Zhang, F. Höflinger, and L. Reindl, “TDOA-based localization using interacting multiple model estimator and ultrasonic transmitter/receiver,” *IEEE Trans. Instrum. Meas.*, vol. 62, no. 8, pp. 2205–2214, Aug. 2013.
- [44] L. Zhao, P. Babu, and D. P. Palomar, “Efficient algorithms on robust low-rank matrix completion against outliers,” *IEEE Trans. Signal Process.*, vol. 64, no. 18, pp. 4767–4780, Sep. 2016.
- [45] M. S. Bazaraa, H. D. Sherali, and C. M. Shetty, *Nonlinear Programming: Theory and Algorithms*, 3rd ed. Hoboken, NJ, USA: Wiley, 2006.
- [46] Z. Yan, J. Fan, and J. Wang, “A collective neurodynamic approach to constrained global optimization,” *IEEE Trans. Neural Netw. Learn. Syst.*, vol. 28, no. 5, pp. 1206–1215, May 2017.
- [47] H. Che and J. Wang, “A two-timescale duplex neurodynamic approach to biconvex optimization,” *IEEE Trans. Neural Netw. Learn. Syst.*, vol. 30, no. 8, pp. 2503–2514, Aug. 2019.
- [48] E. Hildebrand, *Introduction to Numerical Analysis*. New York, NY, USA: Dover, 1987.
- [49] A. Ben-Tal and A. Nemirovski, *Lectures on Modern Convex Optimization: Analysis, Algorithms, and Engineering Applications*, Philadelphia, PA, USA: SIAM, 2001.
- [50] Y. Qi, H. Kobayashi, and H. Suda, “Analysis of wireless geolocation in a non-line-of-sight environment,” *IEEE Trans. Wireless Commun.*, vol. 5, no. 3, pp. 672–681, Mar. 2006.
- [51] M. Grant and S. Boyd, “CVX: MATLAB software for disciplined convex programming, version 2.1.” [Online]. Available: <http://cvxr.com/cvx>